Water SA 50(2) 166–178 / Apr 2024
https://doi.org/10.17159/wsa/2024.v50.i2.4078

Research paper

Degradation of methyl orange by the Fenton-like reaction of pyrite-activated hydrogen peroxide forming the Fe(III)/Fe(II) cycle

Wenlong Bi[1], Ruojin Du[1], Hui Liu[1], Peng Fu[1] and Zhenguo Li[1]

[1]*College of Resources and Environment, Shanxi Agricultural University, Shanxi, 030801, PR China*

In this study, the typical azo dye methyl orange (MO) was degraded by pyrite (FeS_2) activated by hydrogen peroxide (H_2O_2). When [MO] = 0.1 mM, [FeS_2] = 2.0 g/L and [H_2O_2] = 22 mM, 96.4% MO was removed in 120 min and the TOC removal rate was higher than 50%. $HO^•$ was the primary radical responsible for MO degradation. In addition, the acid condition promoted the degradation of MO in the FeS_2/H_2O_2 system. MO in tap water and river water was not effectively degraded, whereas acidification could weaken the inhibitory effect on the FeS_2/H_2O_2 system to enable the degradation of MO in tap and river water. The OD_{600} indicated that the solution was environmentally friendly after the reaction, and three degradation pathways of MO were discussed. In summary, Fe(II) could be dissolved from FeS_2, which activated H_2O_2 to generate Fe(III) and $HO^•$. FeS_2 could reduce Fe(III) into Fe(II), thus realizing the Fe(III)/(II) cycle and efficiently activating H_2O_2 to degrade MO.

CORRESPONDENCE
Wenlong Bi

EMAIL
jiayangbihu@126.com

DATES
Received: 14 May 2023
Accepted: 22 March 2024

KEYWORDS
pyrite
hydrogen peroxide
methyl orange
advanced oxidation processes

INTRODUCTION

With the rapid development of printing and dyeing textile industries, the large amount of printing and dyeing wastewater produced has become one of the main water pollution sources in the world (Gu et al., 2021; Pinedo-Hernández et al., 2022). Printing and dyeing wastewater has a complicated composition, high concentration of pollutants, poor biochemical properties, and is difficult to treat (Ben Hafaiedh et al., 2020; Domingues et al., 2019; Shukla and Remya, 2021). Among the contaminants, methyl orange (MO) contains –N=N– and is a typical azo dye (Aghdasinia et al., 2016; Liu et al., 2022). Wastewater containing MO is discharged into the environment from industrial processes such as textiles and printing, and without effective treatment can have a serious impact on the environmental safety of surrounding water and soil, endangering human health (Giannakis et al., 2021). The accumulation of MO in water reduces the penetration of sunlight, inhibits the growth of aquatic organisms, and leads to an imbalance in the ecosystem (Song et al., 2022). Therefore, the study of efficient treatment methods for methyl orange wastewater has great significance.

Advanced oxidation processes (AOPs) are used to oxidize macromolecular refractory organics into environmentally friendly small molecules by generating free radicals with strong oxidizing properties through electricity, ultraviolet light, and ultrasound (Liu et al., 2022; Peng et al., 2019; Shao et al., 2020). AOPs, such as the Fenton reaction which involves reacting Fe^{2+} with H_2O_2 to produce hydroxyl radical ($HO^•$), have a strong oxidation capacity, a fast reaction rate, high mineralization potential, and simple operation (Almeida et al., 2021; Gorozabel-Mendoza et al., 2021; Zhao et al., 2020). However, the Fenton system has a high catalyst dosage and low pH after reaction (Jin et al., 2021). In addition, the high iron content of $FeSO_4$ added to the Fenton system greatly increases the iron sludge treatment intensity and the disposal cost (Guo et al., 2020; Martins et al., 2017). Therefore, finding a low-cost and environmentally friendly catalyst to replace Fe(II) is critical for advanced oxidation processes.

To solve the iron-rich sludge problem in the Fenton system, a cheap and easily available iron-containing mineral needs to be found to replace ferrous ions. A promising candidate is pyrite (FeS_2), which is the most abundant sulfide mineral on earth. FeS_2 has been shown to be an efficient catalyst for the degradation of alachlor by Fenton's reagent (Kayan et al., 2020), and a nano-pyrite Fenton system was demonstrated to have improved the production of $HO^•$, resulting in the degradation of p-nitrophenol being three times faster than with the traditional Fenton system (Liu et al., 2020). Moreover, FeS_2 is a low-cost, easily available, and environmentally friendly catalyst (Wang et al., 2021). The most noteworthy attribute of FeS_2 is that the resource utilization of FeS_2 can reduce the risk of FeS_2 producing acidic mine wastewater (AMD) (Xia et al., 2023).

Therefore, in this study, FeS_2 was used as a catalyst to explore the degradation and mechanism of MO in FeS_2/H_2O_2 system. Furthermore, considering that printing and dyeing enterprises use a lot of tap water and river water, the degradation of MO in distilled water, tap water, and river water in FeS_2/H_2O_2 system was investigated.

MATERIALS AND METHODS

Chemicals

Methyl orange (MO, $C_{14}H_{14}N_3SO_3Na$, >98.8%) was purchased from Tianjin Tianli Chemical Reagent Co., Ltd. Hydrogen peroxide (H_2O_2, ≥30%) and concentrated sulfuric acid (H_2SO_4, 95.0%~98.0%) were purchased from Chengdu Kolon Chemical Reagent Co., Ltd. Ferrous sulfate ($FeSO_4·7H_2O$, ≥99.0%), sodium hydroxide (NaOH, 96.0%), methanol (CH_3OH, ≥99.5%), and tert-butyl alcohol (TBA, $(CH_3)_3COH$, ≥99.5%) were purchased from Tianjin Beichen Founder Reagent Factory. All the above reagents were analytically pure. All aqueous solutions were prepared with distilled water.

Pyrite pretreatment

Natural pyrite (FeS_2) was purchased from Hebei China. Pyrite was ground and passed through a 0.15 mm mesh sieve, placed in a beaker and soaked in 0.5 M H_2SO_4 solution for 1 h to remove impurities and then filtered. The pyrite was washed repeatedly with distilled water until the pH of the filtrate was 7, and then filtered. The filtered sample was dried in an oven at about 40°C for future use.

Experimental method

MO removal by pyrite alone or hydrogen peroxide alone

FeS_2 (0.2–2.0 g/L) or H_2O_2 (30–50 mM) was added to MO (0.1 mM) and the solution placed on a magnetic stirrer; 3 mL samples were taken at 5, 10, 20, 30, 60, 90, and 120 min and then to each sample 0.5 mL of MeOH was added, which can quench free radicals to ensure sample stability. The concentration of MO was calculated by colorimetric measurement at 470 nm (iso-absorption point wavelength, which is the wavelength at the intersection of the acidic and alkaline absorption curves) with a 721 visible spectrophotometer.

Optimization of pyrite and hydrogen peroxide

The addition of FeS_2 and H_2O_2 was optimised using the response surface method in Design-Expert software. The design of experiment (DOE) is given in Table 1 which was designed using response surface methodology (RSM) (Ebru et al., 2023). The initial concentration of MO was 0.1 mmol/L, and the software-designed doses of FeS_2 and H_2O_2 were added sequentially before the start of the reaction. 3 mL of the sample was removed from the filtrate at 15, 30, 45 and 60 min by passing it through a 0.45 μm membrane and adding 0.5 mL of methanol (free radical scavenger), and the concentrations were measured using a 721 visible spectrophotometer. The pH and temperature of the solution was measured at the end of the reaction. The data were visualised and analysed in Design-Expert software to obtain the optimum dose of FeS_2 and H_2O_2.

Effect of different factors

In pH-effect experiments, the pH of the MO (0.1 mM) solution was adjusted to 2, 4, 6, 8 and 10 with H_2SO_4 and NaOH, respectively, and then FeS_2 and H_2O_2 were added after the above optimization. The reaction was started and timed at 5, 10, 20, 30, 60, 90 and 120 min. 3 mL of the sample was removed from the filtrate after passing through a 0.45 μm filter membrane and 0.5 mL of methanol was added. The concentrations were measured using a 721 visible spectrophotometer, and the pH and temperature of the solution were measured at the end of the reaction. In the free-radical-contribution experiment, 2 mL TBA was added to MO solution, after adding optimized FeS_2 and H_2O_2 into the MO solution; the remaining experimental steps were as above. All water used in the above procedures was distilled water. The influence experiment for different water matrices was conducted using distilled water, tap water, and river water (the Uma River in Taigu) to prepare MO solutions for degradation experiments, and the remaining experimental steps were performed as above.

Table 1. Design of experiment and removal efficiency of MO

No.	Mode	Addition		Response
		FeS_2 (g/L)	H_2O_2 (mmol/L)	Removal efficiency (%)
1	−−	0.2	2	1.2
2	a0	0.2	16	4.9
3	−+	0.2	30	4.2
4	0a	1.1	2	2.5
5	00	1.1	16	91.9
6	00	1.1	16	92.0
7	0A	1.1	30	19.6
8	+−	2.0	2	8.4
9	A0	2.0	16	88.9
10	++	2.0	30	93.2

Table 2. Composition of the medium

Composition	Content (mg/L)
KNO_3	1 900
NH_4Cl	1 100
KH_2PO_4	170
$MgSO_4$	370
$CaCl_2$	440
$C_6H_{12}O_6$	2 000
Peptones	300

Biotoxicity experiments

Biotoxicity experiments used microbial communities obtained by isolation and activation from campus soil (the soil was taken to cultivate the microorganisms used in the experiment in the area where the vegetation on the campus was lush and the microorganisms were active). The composition and content of the medium is given in Table 2. The 15 mL reaction solution was added to 10 mL of the medium and 0.5 mL mixed microbial community solution, and placed in an oscillator (rotating speed 180 r/min, temperature 25°C) for oscillating culture. Samples were taken at 6, 9, 12, 24 and 48 h, and the OD_{600} value reflecting bacterial density was determined by spectrophotometer. According to the difference between the reaction solution and the blank treatment, the microbial toxicity of the treatment solution was determined.

Analysis methods

Determination of total organic carbon concentration was conducted using a total organic carbon analyser (TOC; Muti N/C-3100 mode1). A scanning electron microscope (SEM; JSM-7001F) and X-ray diffractometer (XRD; MiniFlex II) were used to characterize FeS_2. FeS_2 surface elements were analysed using Al-Kα monochromatic X-ray photoelectron spectroscopy (XPS; AXIS ULTRA DLD). The intermediate products of MO degradation were analysed by a liquid chromatography–mass spectrometer (LC-MS; Agilent 1290 II-6470).

RESULTS AND DISCUSSION

Removal of MO by FeS_2 alone and H_2O_2 alone

The removal effect for MO by different concentrations of FeS_2 was examined as shown in Fig. 1a. When the FeS_2 concentration was in the range of 0.2–2.0 g/L, the adsorption capacity of FeS_2 for MO was weak and fluctuated up and down in the range of 0–3.5%. With an increase in FeS_2 concentration, adsorption of MO did not improve effectively. Figure 1b shows the removal effect for MO by different concentrations of H_2O_2. The removal rates of MO at 30, 40 and 50 mmol/L H_2O_2 after 150 min were 2.8%, 5.0% and 4.9%, respectively. As the concentration of H_2O_2 increased, removal of MO did not increase significantly, indicating that the oxidation of MO by H_2O_2 was weak.

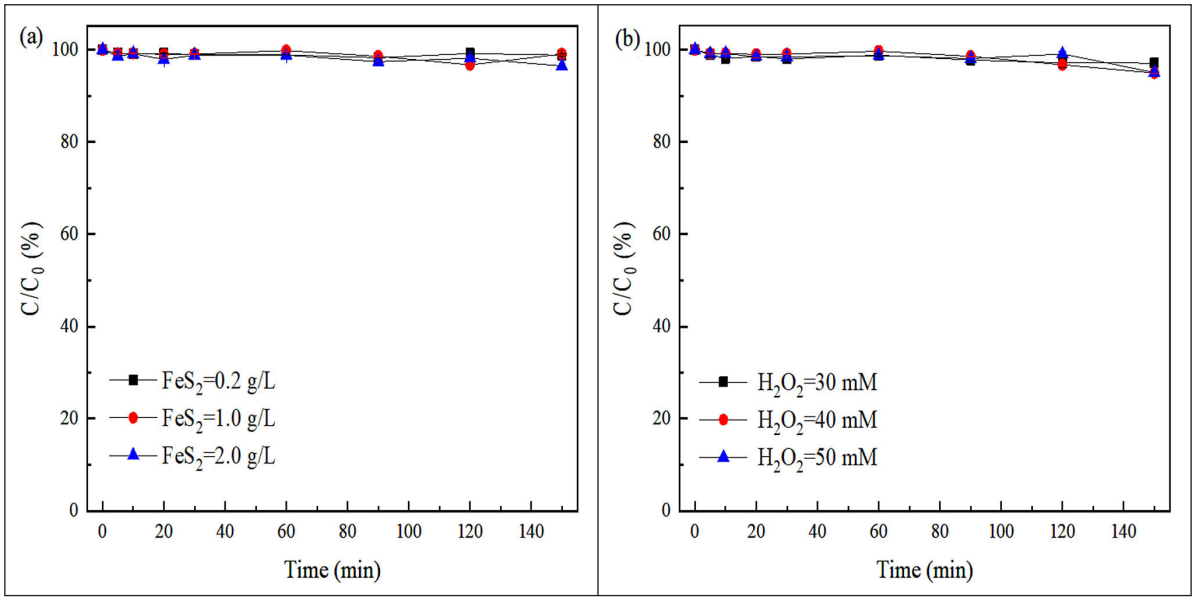

Figure 1. Removal of MO by FeS_2 alone (a) and H_2O_2 alone (b); [MO] = 0.1 mM, T = 25°C, without pH adjustment

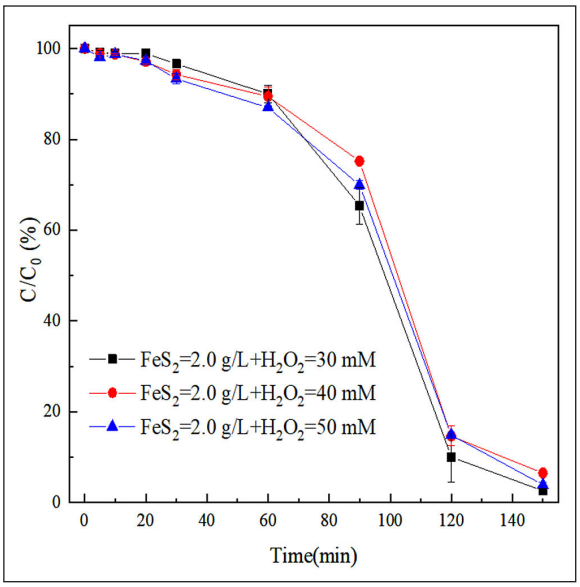

Figure 2. The degradation of MO in FeS_2/H_2O_2 with different concentrations of H_2O_2; [MO] = 0.1 mM, [FeS_2] = 2.0 g/L, T = 25°C, without pH adjustment

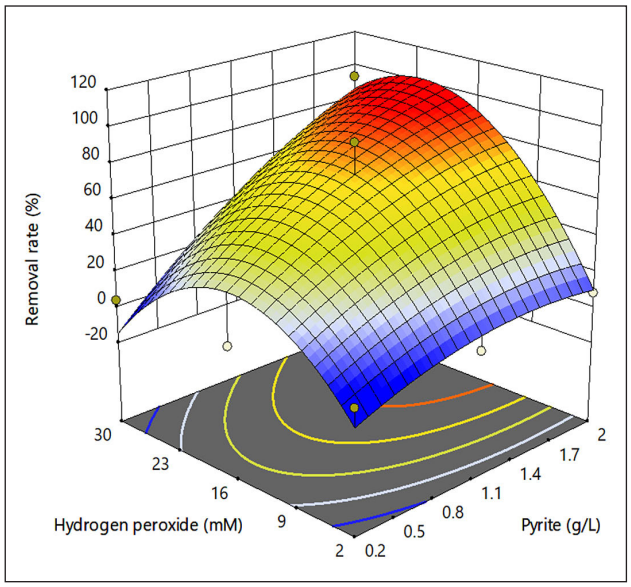

Figure 3. 3D surface plot of MO removal rate after 150 min by the interaction between FeS_2 and H_2O_2 concentration; $[MO]_0$ = 0.1 mM, T = 25°C, without pH adjustment

The degradation of MO in FeS_2/H_2O_2 with different concentrations of H_2O_2

As can be seen from Fig. 2, when 0.1 mmol/L MO and [2.0 g/L FeS_2 were added, the residual of MO at 30, 40 and 50 mmol/L H_2O_2 after 150 min of reaction was 97.4%, 93.5% and 96.1%, respectively. The degradation rate of MO was significantly increased after the simultaneous addition of FeS_2 and H_2O_2. This may be due to the continuous dissolution of Fe(II) from FeS_2 and the continuous activation of H_2O_2 by Fe(II) to produce HO• (Eq. 1) to degrade MO (Oral and Kantar, 2019). Moreover, the sulfide in FeS_2 could reduce Fe(III) to Fe(II) (Eq. 2) (Liu et al., 2015), further promoting the Fenton-like reaction. With the increase in H_2O_2 concentration, the difference between the removal rates for methyl orange was only 3.9%. Excluding the interference of error lines and combined with the desire for 'green and efficient', a relatively low concentration of H_2O_2 (30 mmol/L) was finally chosen for the subsequent optimization experiments.

$$Fe(II) + H_2O_2 \rightarrow Fe(III) + OH^- + HO^\bullet \quad (1)$$

$$FeS_2 + 14Fe(III) + 8H_2O \rightarrow 15Fe(II) + 2SO_4^{\bullet-} + 16H^+ \quad (2)$$

Determination of the optimal concentration of FeS_2 and H_2O_2

Response surface method optimization

By analysing the results of MO removal by FeS_2 alone, H_2O_2 alone, and FeS_2/H_2O_2 system (Figs 1 and 2), the concentration ranges of FeS_2 and H_2O_2 were determined, and then 3D surface plots of MO removal rate after 150 min were fitted by Design-Expert software for the interaction between FeS_2 and H_2O_2 concentrations (Abd Manan et al. 2019). As can be seen from Fig. 3, when the MO concentration was 0.1 mM, H_2O_2 concentration was 22 mM, and FeS_2 concentration was 2.0 g/L, the MO removal rate was expected to reach 100% after 150 min.

The MO removal rate increased with the increase in FeS_2 concentration. This was probably due to the degradation of MO with the increased FeS_2 that could dissolve more Fe(II)-activated H_2O_2, generating $HO^•$ production.

When the MO concentration was 0.1 mM, FeS_2 concentration was 2.0 g/L, and with the increase in H_2O_2 concentration, the MO removal rate showed a trend of first increasing and then decreasing. The MO removal rate increased with the increase in H_2O_2 concentration in the range of 0–22 mM, which may be due to Fe(II) dissolved from FeS_2, then reacting with H_2O_2 to generate $HO^•$. However, MO removal decreased once the H_2O_2 concentration was above 22 mM. On the one hand, H_2O_2 is a capture agent for $HO^•$, and excess H_2O_2 would not only react with Fe(II), but also with $HO^•$ to produce $HO_2^•$ with low activity (Eq. 3) (Chang et al., 2020; Sun et al., 2019; Xiao et al., 2020), making the reaction rate decrease. On the other hand, excess $HO^•$ would react not only with the target substance but also with Fe(II), which made the degradation rate of MO decrease.

$$HO^• + H_2O_2 \rightarrow HO_2^• + H_2O \quad (3)$$

Verification of optimal conditions

To verify the above response surface methodology optimization results, the MO removal by different systems was plotted in Fig. 4a. MO removal by FeS_2 or H_2O_2 alone was minimal. After 150 min of reaction, the MO removal by FeS_2 alone was only 3.5%, and FeS_2 had no obvious oxidative adsorption effect on MO. The MO removal rate by H_2O_2 alone was only 4%, so the oxidation effect of H_2O_2 on MO was weak.

When the MO concentration was 0.1 mM, H_2O_2 concentration was 22 mM, and FeS_2 concentration was 2.0 g/L, the MO removal rate reached 96.3% at 120 min. The MO removal rate showed a trend of plateau, then a high rate, and finally a plateau again, which is consistent with a traditional Fenton-like trend (Wang et al., 2013; Yan et al., 2017). The rapid degradation of MO at the stage of 30–90 min may be due to Fe(II) being dissolved from FeS_2, which then reacted with H_2O_2 to produce $HO^•$. FeS_2 also reduced Fe(III) to Fe(II), which continues to react with H_2O_2, resulting in rapid degradation of MO. The results for the UV scanning spectrum at different times also indicated rapid degradation of MO within 30–90 min (Fig. 4b). During the 90–150 min stage, the degradation of MO was slow. On the one hand, H_2O_2 was gradually consumed in FeS_2/H_2O_2 system (Kokilavani et al., 2021), which made only a small amount of H_2O_2 react with Fe(II). On the other hand, intermediates of MO would compete with MO for $HO^•$, slowing the MO degradation rate. To sum up, compared with FeS_2 alone or H_2O_2 alone, the FeS_2/H_2O_2 system could significantly remove MO. In addition, the degradation of MO tends to level off after 120 min. Because the concentration of MO at 150 min remained almost unchanged compared to that at 120 min, the final sampling time for subsequent experiments was 120 min.

Table 3 shows MO removal rates by other activated H_2O_2 methods. In Fe(II)/H_2O_2 system, although the MO is degraded in a short time, the amount of Fe(II) is large and the cost is high.

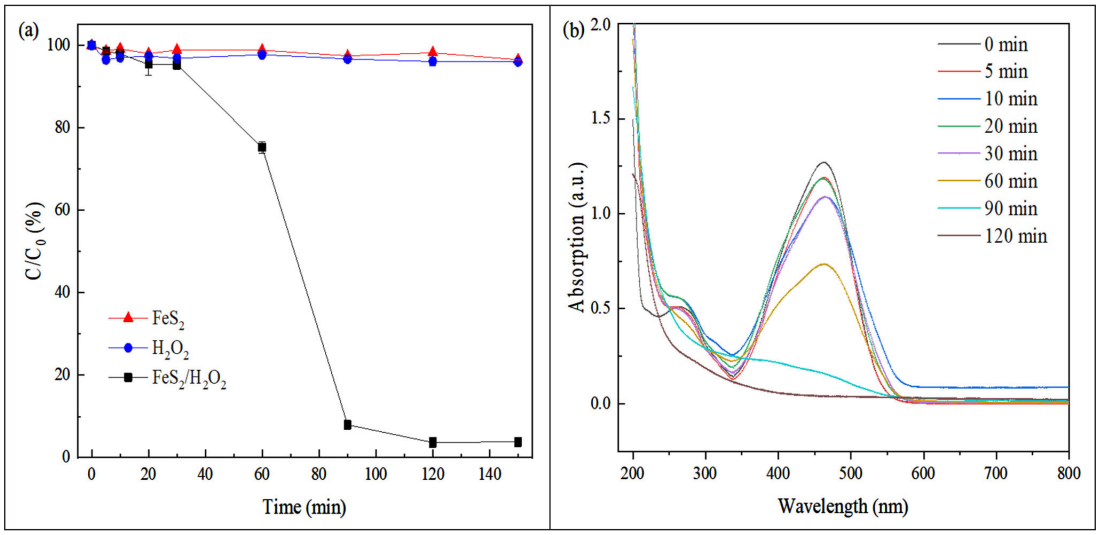

Figure 4. The degradation of MO in different systems (a) and UV spectrum of MO degraded at different time points in FeS_2/H_2O_2 system (b); $[MO]_0 = 0.1$ mM, $[FeS_2]_0 = 2.0$ g/L, $[H_2O_2]_0 = 22$ mM, $T = 25$°C, without pH adjustment

Table 3. Methyl orange removal rates by other activated H_2O_2 methods

Activation method	H_2O_2 concentration (mM)	Reaction time (min)	MO concentration (mM)	Additional conditions	Removal rate	Reference
Fe(II)/H_2O_2	2.93	15	0.054	[Fe(II)] = 10.64 mg/L; initial pH = 6.69	86.25%	Youssef et al., 2016
Fe(II)/H_2O_2	1	8	0.1	[Fe(II)] = 22.4 mg/L; initial pH = 3.3	91.8%	Zhiyong et al., 2013
UV/H_2O_2	45.8	3	0.078	$P_0 = 26.9$ mW	100%	Haji et al., 2011
UV/H_2O_2	91.1	8	0.078	$P_0 = 26.14$ mW	100%	Haji et al., 2014
Fe(III)-Y zeolite/H_2O_2	91.1	60	0.078	[Fe-Y zeolite] = 9.9 g/L	82%	Haji et al., 2014
MIL–100(Fe)/GO/H_2O_2	8	240	0.15	[MIL–100(Fe)/GO] = 0.5 g/L; pH = 3.0; $T = 30$°C	98%	Tang and Wang, 2017
Siderite/H_2O_2	60	720	0.15	[siderite] = 2.5 g/L; $T = 25$°C; initial pH = 7.0	~10%	Song et al., 2022
FeS_2/H_2O_2	22	120	0.1	[FeS_2] = 2 g/L; initial pH = 5.97	96.3%	This study

In UV/H_2O_2 system, an additional light source is needed and a large amount of H_2O_2 is required. Compared with other iron-based/H_2O_2 systems, FeS_2/H_2O_2 system could efficiently degrade 96.3% of MO with low doses of FeS_2 and H_2O_2. In addition, FeS_2 is a mineral that exists in nature, is low cost and easy to obtain, and has good application value.

Contribution of different factors to FeS_2/H_2O_2 system

Concentration of total Fe and Fe(II)

Fe(II) plays a catalytic role in FeS_2/H_2O_2 system, which could activate H_2O_2 to generate HO• and effectively degrade MO, and all iron ions in this system originate from FeS_2. Therefore, we measured the total Fe and Fe(II) concentrations in FeS_2/H_2O_2 system as shown in Fig. 5a. The total Fe concentration increased with time, but all of the concentrations recorded were lower than 3.5 mg/L. The Fe(II) concentration fluctuated from 0.33–0.64 mg/L. After 30 min of reaction, the total Fe and Fe(II) concentrations were 0.43 mg/L and 0.33 mg/L respectively, indicating that the slow degradation of MO in FeS_2/H_2O_2 system before 30 min was due to the slow dissolution of Fe ions. During 30–120 min, the total Fe content increased significantly, reaching 3.12 mg/L at 120 min, while Fe(II) did not increase, reaching 0.64 mg/L at 120 min. This may be due to the rapid reaction of dissolved Fe(II) with H_2O_2 to form Fe(III), FeS_2 could reduce Fe(III) to Fe(II), and the reaction rate of Eq. 1 is faster than that of Eq. 2 (Diao and Chu 2021). Therefore, there was a large amount of Fe(III), and Fe(II)/Fe(III) in dynamic states, in the system, confirming that the degradation of MO was rapid after 30 min in FeS_2/H_2O_2 system.

Validation of the interface effect of pyrite

H_2O_2 and Fe(II) were added to the MO solution to form Fe(II)/H_2O_2 homogeneous system to investigate the interface effect of FeS_2. It can be seen from Fig. 5b that MO degraded slowly in Fe(II)/H_2O_2 system, and the degradation rate of MO was 77.4% after 120 min. H_2O_2 rapidly produced a large amount of HO• under the action of a high concentration catalyst in the early stage (Dulova et al., 2017). However, due to the limited reaction rate of HO• with organic matter, the free HO• not participating in the reaction aggregates, and free HO• reacted with itself to form H_2O, resulting in a part of the initially generated HO• being wasted (Liu et al., 2021). Furthermore, there were a large number of intermediate products of MO in the system, which might compete with MO for HO•. Therefore, the degradation trend of MO tended to level off. The pH after the reaction of the Fe(II)/H_2O_2 and FeS_2/H_2O_2 systems was 4.00 and 3.25, respectively. FeS_2 has the advantages of low cost and easy availability, so it has good application prospects.

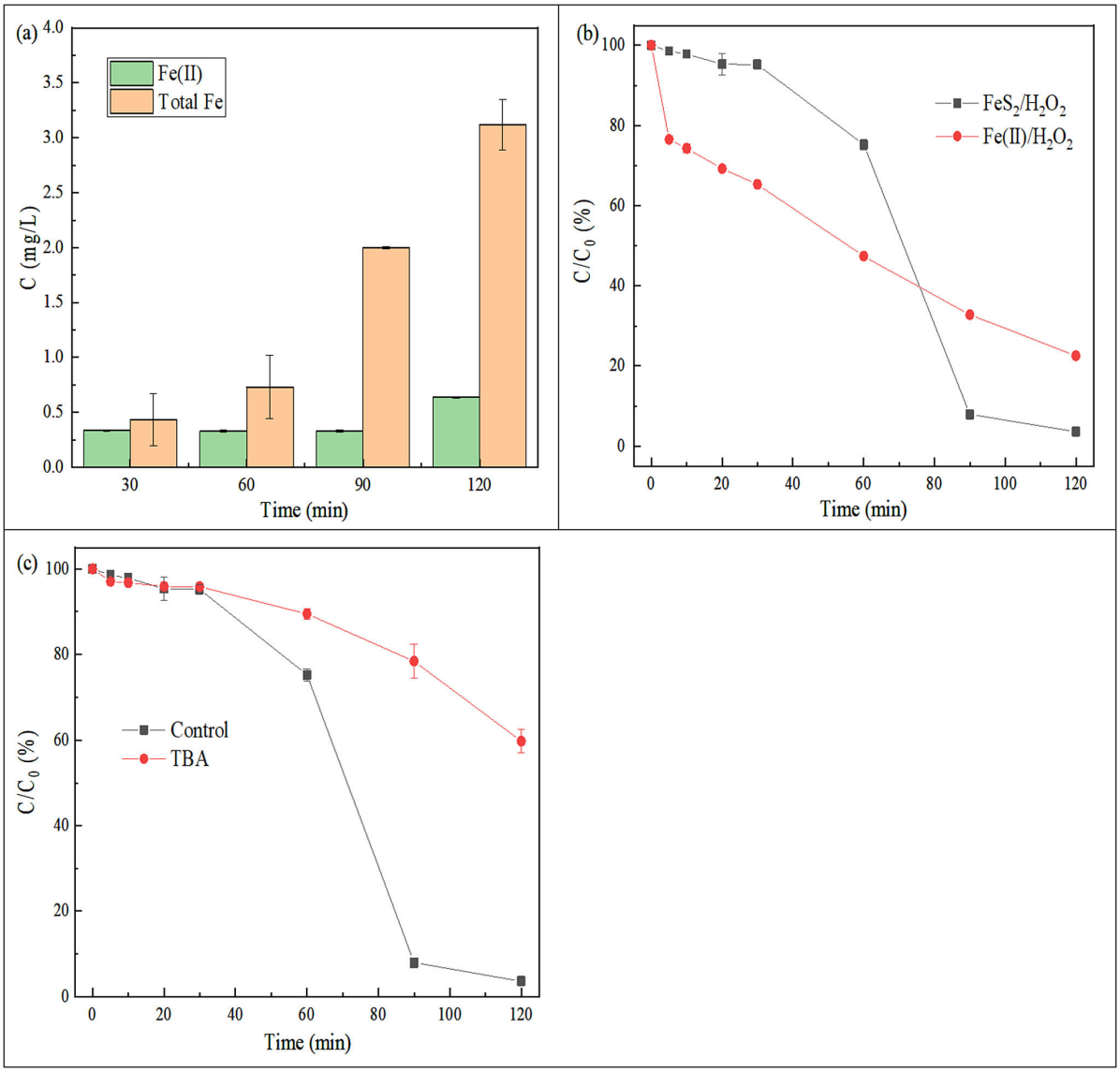

Figure 5. Determination of total Fe and Fe(II) (a), verification of interfacial effects of FeS_2 (b), free radical contribution (c) in FeS_2/H_2O_2 system; $[MO]_0$ = 0.1 mM, $[FeS_2]_0$ = 2.0 g/L, $[Fe(II)]_0$ = 3 mg/L, $[H_2O_2]_0$ = 22 mM, T = 25°C, without pH adjustment

Free radical contribution

To investigate the reactive oxygen species that played a dominant role in the removal of MO from FeS_2/H_2O_2 system, a certain amount of free radical scavenger was added to the reaction system. The reaction rate constants of tert-butanol (TBA) and HO• are (3.8~7.6) × 10^8 M/s, so TBA is commonly used as a HO• scavenger (Chen et al. 2021, Xu and Sheng 2021). In addition, to effectively quench HO• within the system, we added TBA (0.4 M) at 4 000 times the dose of MO (0.1 mM). The effect of TBA on the degradation of MO in FeS_2/H_2O_2 system is shown in Fig. 5c. The addition of TBA significantly inhibited the degradation of MO, and the MO removal rate was only 40.2% in 120 min. Therefore, HO• was the dominant reaction species in the system, and its contribution to the degradation of MO was about 58.3%. The interfacial effect of FeS_2 also contributed as the added FeS_2 particle interface reacted with H_2O_2.

Influence of pH on the degradation of MO in FeS_2/H_2O_2 system

The degradation of MO in FeS_2/H_2O_2 system under different pH levels was shown in Fig. 6. In FeS_2/H_2O_2 system, MO could be effectively removed under neutral and acidic conditions, and the removal effect was better under acidic conditions (Jin et al., 2021). However, it was difficult to effectively remove MO at pH = 10.

When the initial pH was 2 and 4, the MO degradation showed a fast and then slow trend. The degradation rates in 0–60 min were fast, and the MO removal rate could reach 94.8% and 87.5% in 60 min. The degradation tends to reach equilibrium within 60–120 min, with an increase of 2.4% and 8.7% in MO removal at 120 min compared with 60 min. Under acidic conditions, the dissolution of Fe(II) in FeS_2 could be promoted (Li et al. 2019). Therefore, in the early stage of the reaction, the Fe(II) would immediately activate H_2O_2, which made MO degrade rapidly. The slow degradation of MO after 60 min may be due to the decrease of H_2O_2, and only a small amount of Fe(II) reacted with a small amount of H_2O_2, which made MO degrade slowly. When the initial pH was 6 and 8, MO removals were 94.0% and 93.0%, respectively, after 120 min. The degradation trends were all flat, then fast and finally flat again, similar to the degradation trends at unadjusted pH (Dos Santos et al., 2021). The rapid degradation of MO in 30–90 min was not only due to the massive dissolution of Fe(II) to produce HO•, but also because FeS_2 would produce H^+ during the reduction of Fe(III), resulting in more dissolution of Fe(II) after the reduction of pH. Under the alkaline condition, the MO removal rate was poor at the initial pH of 10, and was only 2.2% after 120 min. It may be that Fe(II) dissolved slowly in FeS_2 under the alkaline condition (Dong et al., 2019).

When the initial pH was 10, the pH after the reaction was 9.71. However, with all of the other starting pH values, the pH after the reaction was less than 4 (Table 4). During the reduction of Fe(III), FeS_2 produces H^+, which lowers the pH of the solution. Under a traditional Fenton system, the best degradation efficiency was achieved at pH 2.79. At an initial pH of 8.0, there was almost no degradation of MO (Youssef et al., 2016). Compared with the traditional Fenton system, the FeS_2/H_2O_2 system has a wider range of pH applications.

Influence of different water matrices on MO degradation in FeS_2/H_2O_2 system

In practice, most printing and dyeing textile industries would directly use tap water or river water for treatment and, after a series of processes, the discharged wastewater has a complex composition. Therefore, we investigated MO degradation in tap water and river water by FeS_2/H_2O_2 system to verify the possibility of FeS_2 treatment toward disposal of actual printing and dyeing wastewater.

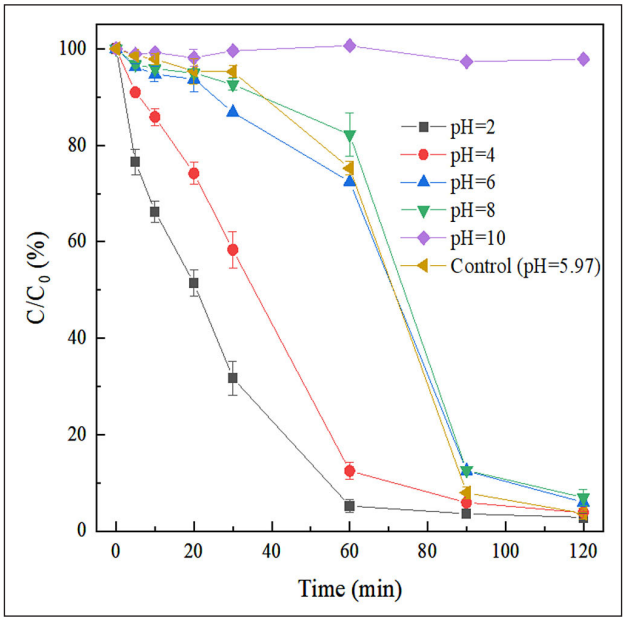

Figure 6. Influence of pH on the degradation of MO in FeS_2/H_2O_2 system; $[MO]_0$ = 0.1 mM, $[FeS_2]_0$ = 2.0 g/L, $[H_2O_2]_0$ = 22 mM, T = 25°C

Table 4. pH before and after the degradation of MO by FeS_2/H_2O_2 system under different pH conditions: [MO] = 0.1 mM, [FeS_2] = 2.0 g/L, [H_2O_2] = 22 mM, 25°C

Condition	pH = 2	pH = 4	pH = 6	pH = 8	pH = 10	Control
Before	1.99	4.00	5.98	8.02	10.03	5.97
After	1.98	3.89	4.00	4.09	9.71	3.25

As shown in Fig. 7a, MO was not effectively degraded in river water and tap water, and its degradation effect was much lower than that in distilled water. By determining the physical and chemical properties of river water and tap water (Table A1, Appendix) it was shown that they were weakly alkaline in pH and all had high TOC content. Consequently, it is speculated that the alkaline water would react with HO• to form low levels of active free radicals (Eqs 4–5) (Jiang et al., 2021; Ma et al., 2018), and the organic matter in river water and tap water would compete with MO for HO•. Hence there was no obvious removal effect for MO.

$$HO^{\bullet} + HCO_3^- \rightarrow HCO_3^{\bullet} + OH^- \quad (4)$$

$$HO^{\bullet} + Cl^- \rightarrow ClHO^{\bullet -} \quad (5)$$

Under the acidic condition, the dissolution of Fe (II) will be accelerated and this will promote MO degradation. Moreover, the acidification could remove CO_3^{2-}, HCO_3^-, Br^-, NO_3^-, and Cl^- in water. The distribution of carbonation binding states in Fig. A1 (Appendix) shows that at pH < 4 there is only free CO_2 in the water. Therefore, the effect of different water matrices at pH = 2 was further investigated (Fig. 7b). After 60 min of reaction, the MO removal rates in distilled water, tap water, and river water were 97.2%, 96.9%, and 97.6%, respectively, achieving the expected treatment effect. Moreover, we prepared MO wastewater with similar ions to the water taken from the Uma River. It was found that the simulated wastewater was difficult to degrade in FeS_2/H_2O_2 system without adjusted pH, whereas the simulated wastewater had good degradation at a pH of 2 (Fig. 8), which further confirmed that acidification could weaken the inhibitory effect on the FeS_2/H_2O_2 system for degrading MO in tap and river water.

Characterization of pyrite before and after reaction

The elemental composition of FeS_2 and the chemical states of Fe and S elements before and after the reaction were analysed by XPS. As can be seen from Fig. 9a, FeS_2 before and after the reaction was mainly composed of S, C, O, Fe, and Na. It could also be detected by EDS spectra (Fig. A2, Appendix). The C and O may be surface oxides, and Fe and S decreased in intensity after use, which may be as a result of being dissolved from the mineral into water. A corresponding change in the relative intensity of FeS_2 before and after the reaction could also be observed by XRD (Fig. 9b).

The high-resolution Fe-2p spectra of FeS_2 is shown in Fig. 9c. The peaks of 707.3, 709.6, 710.8, 711.5, and 714.2 eV of Fe $2p_{3/2}$ orbit were FeS_2, FeO, Fe_2O_3, FeOOH, and satellite peaks, respectively. Except for the satellite peak, the peak area ratios before reaction were 40.2%, 10.7%, 23.6%, and 25.5%, respectively. The FeS_2 peak area decreased by 8.9%, while the FeOOH peak area increased by 8.7% after the reaction.

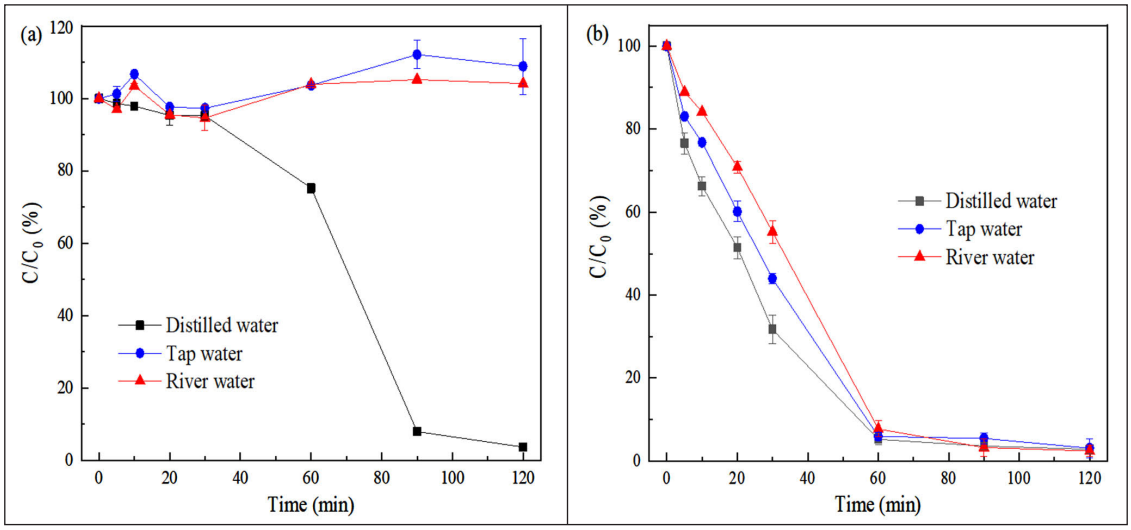

Figure 7. Influence of different water matrices on MO degradation in FeS_2/H_2O_2 system without the adjustment of pH (a) and pH = 2 (b); $[MO]_0$ = 0.1 mM, $[FeS_2]_0$ = 2.0 g/L, $[H_2O_2]_0$ = 22 mM, T = 25°C

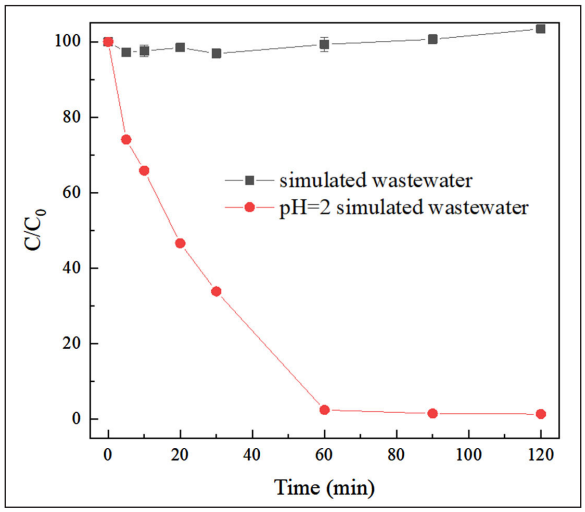

Figure 8. Effect of simulated wastewater on the degradation of MO in FeS_2/H_2O_2 system.
$[MgSO_4]$ = 10 mM, $[CaCl_2]$ = 0.5 mM, [KCl] = 0.5 mM, $[NaHCO_3]$ = 2.5 mM, [MO] = 0.1 mM, $[FeS_2]$ = 2.0 g/L, $[H_2O_2]$ = 22 mM

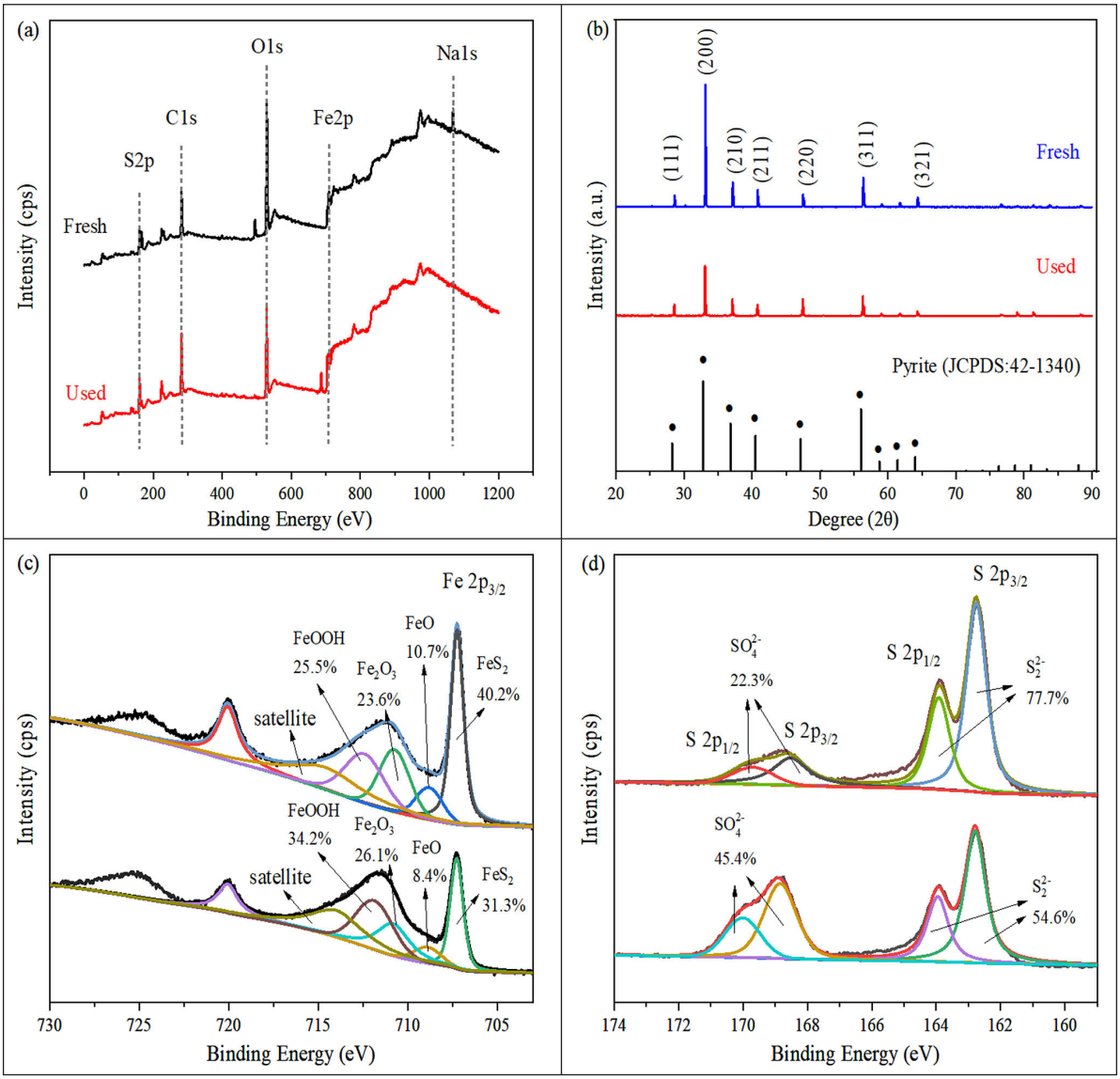

Figure 9. XPS full spectrum (a), XRD (b), and high-resolution spectra of Fe (c) and S (d) of FeS_2 before and after the reaction

As can be seen from Fig. 9d, the peaks at 162.6 and 163.9 eV correspond to the S $2p_{3/2}$ and S $2p_{1/2}$ orbitals of S_2^{2-} (Ye et al., 2021). The peak area of S_2^{2-} decreases from 77.7% to 54.6% before and after the reaction. The peaks at 168.5 and 169.7 eV are the S $2p_{3/2}$ and S $2p_{1/2}$ orbitals of SO_4^{2-}, and the peak area of SO_4^{2-} increased by 23.1% before and after the reaction. This indicates that S_2^{2-} in FeS_2 was oxidized to SO_4^{2-} during the oxidation process, which was consistent with the reaction given in Eq. 2 (Gao et al., 2021). Since the conversion of elemental S was much larger than that of elemental Fe, it was speculated that sulfide in FeS_2 could promote the conversion of Fe(III) to Fe(II) (Yu et al., 2020).

Determination of biotoxicity and total organic carbon of MO degraded by FeS_2/H_2O_2 system

The growth of microorganisms was observed by determining the OD_{600} value to assess the biotoxicity of the FeS_2/H_2O_2 system's degradation of MO. As can be seen from Fig. 10a, during 0–12 h, the number of microorganisms in the FeS_2/H_2O_2 system was more than that in distilled water and MO solution. However, the biotoxicity of FeS_2/H_2O_2 system at 48 h was not significantly different from that of MO, further suggesting that the FeS_2, H_2O_2 and intermediate degradation products of MO were environmentally friendly. Thus, there is an excellent application prospect.

The total organic carbon (TOC) concentration in the FeS_2/H_2O_2 system was measured to observe the degradation of MO (Suave et al., 2018). The TOC removal rate increased with increasing reaction time (Fig. 10b), indicating that the total carbon content in MO wastewater gradually decreased with time (Hamad et al., 2016). In FeS_2/H_2O_2 system, the TOC removal rate reached 58.8% after 2 h of reaction. In summary, the FeS_2/H_2O_2 system was capable of effectively degrading MO.

Possible degradation pathways and mechanism of MO in FeS_2/H_2O_2 system

To determine the degradation path of MO, LC-MS was used to analyse the degradation intermediates of MO. Figure A3 (Appendix) shows the liquid-phase mass spectra of MO at 120 min; 8 intermediates of MO were inferred, and their molecular structures are listed in Table A2 (Appendix). The degradation pathways are shown in Fig. 11a. In FeS_2/H_2O_2 system, Na of MO generally existed in the form of ion, and MO degradation paths were roughly divided into two: one was demethylation and deaminization for P1, P5, and P6 products; P7 was the –N=N– breakage product (Zhang et al., 2020), and P3 and P8 were deaminization products. Pathway 2 was that MO first broke the N=N– to P2, further –NH–NH– broke to P3, P4, and eventually became other small molecules. Figure 11b shows the degradation

mechanism for MO in FeS_2/H_2O_2 system. Fe(II) dissolved from FeS_2, and Fe(II) activated H_2O_2 to generate $HO^{\bullet}$, while sulfide in FeS_2 could reduce Fe(III) to Fe(II) and continuously activate H_2O_2 to generate $HO^{\bullet}$ for MO degradation.

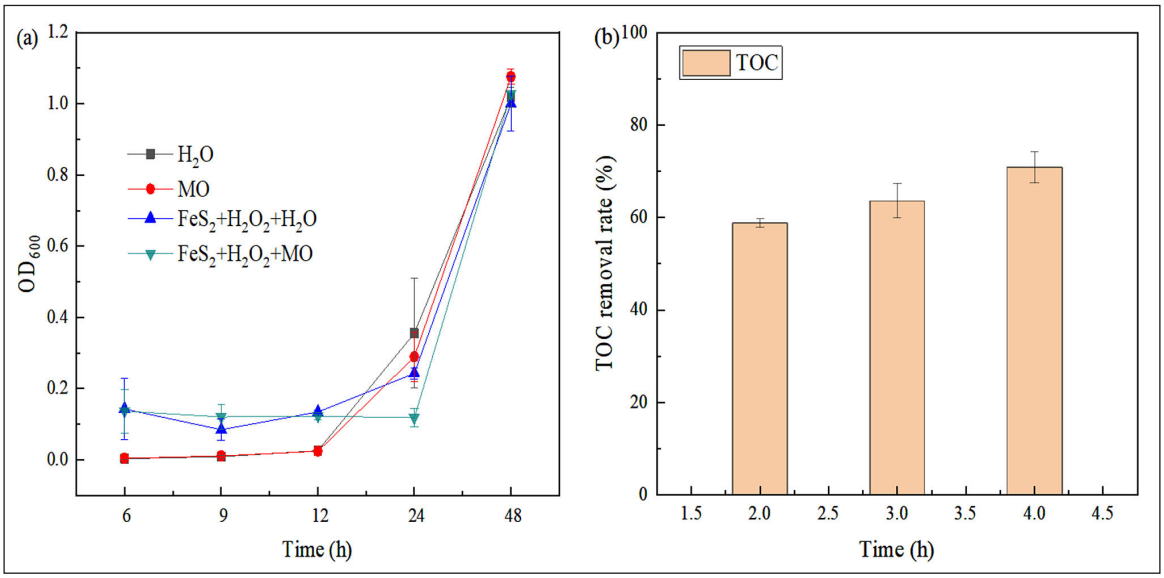

Figure 10. Biotoxicity (a) and TOC removal (b) of MO degraded by FeS_2/H_2O_2; $[MO]_0 = 0.1$ mM, $[FeS_2]_0 = 2.0$ g/L, $[H_2O_2]_0 = 22$ mM, $T = 25$°C, without pH adjustment

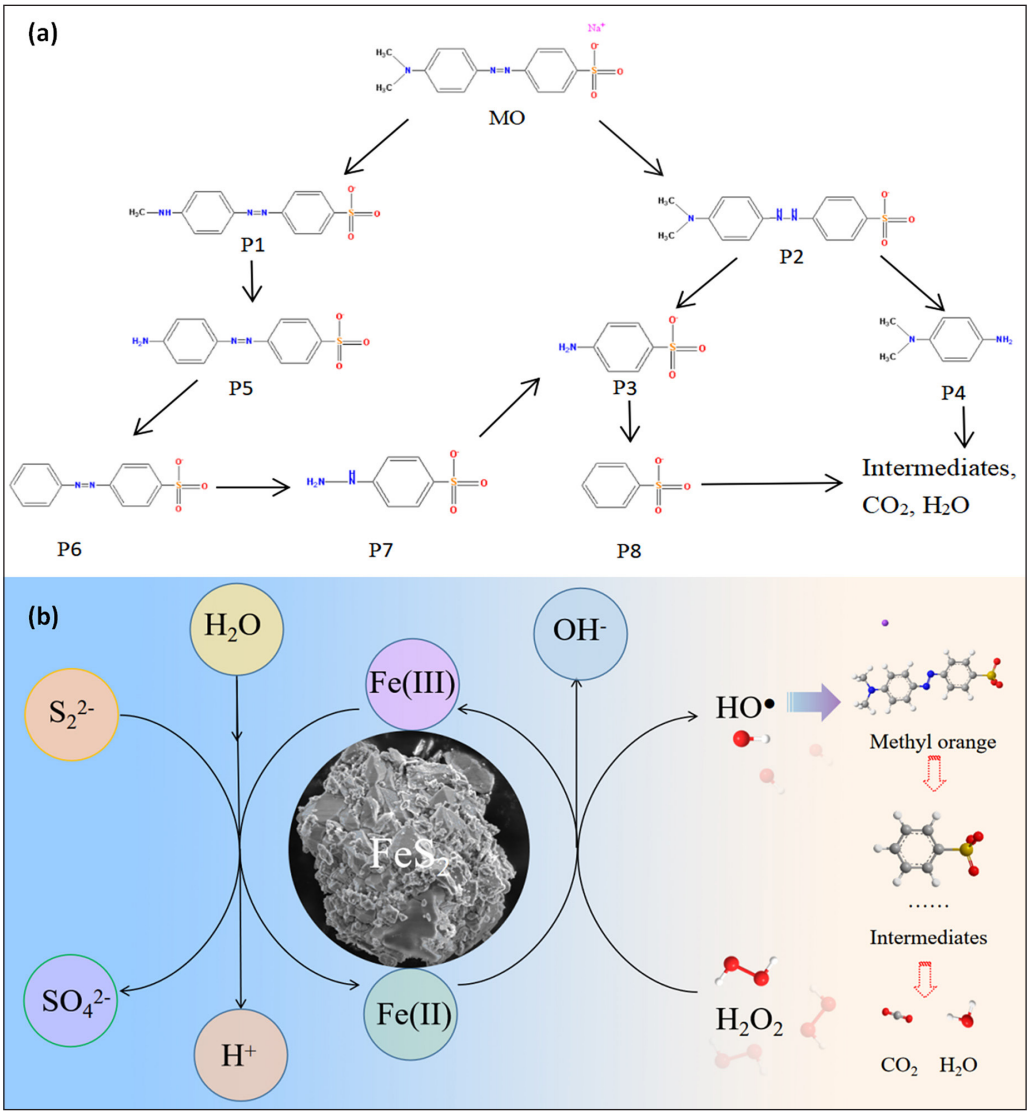

Figure 11. The possible degradation pathways (a) and mechanism (b) of MO in FeS_2/H_2O_2 system

CONCLUSION

In this study, H_2O_2 activated by FeS_2 was effective in degrading MO and HO• was the main radical. In addition, the removal rate of TOC was higher than 50%. In addition, the reaction solution was environmentally friendly and three possible pathways for the degradation of MO were analysed. Compared with the traditional Fenton system, the FeS_2/H_2O_2 system has a wider range of pH applications. Furthermore, MO in tap water and river water could not be effectively degraded in FeS_2/H_2O_2 system. However, acidity could promote MO degradation; hence MO in tap water and river water at pH = 2 was rapidly degraded within 60 min. The degradation mechanism was that Fe(II) dissolved from FeS_2, Fe(II) activated H_2O_2 to generate HO•, which could degrade MO. Meanwhile, FeS_2 could reduce Fe(III) to Fe(II). Therefore, the Fe(III)/Fe(II) cycle formed could continuously activate H_2O_2 to produce HO• to degrade MO.

AUTHOR CONTRIBUTIONS

The manuscript was written by Hui Liu. Ruojin Du contributed to the preparation and review of this manuscript. Experiments were performed by Peng Fu, and data analyses were carried out by Zhenguo Li. The project was supervised by Wenlong Bi. All authors have read and agreed to the published version of the manuscript.

ACKNOWLEDGEMENTS

This work was supported by the Youth Foundation of Shanxi Agricultural University Science and Technology Innovation Enhancement Project (CXGC2023026). Thanks to the staff of the College of Resources and Environment, Shanxi Agricultural University, and we are grateful to the anonymous reviewers and the editors for their valuable suggestions and comments on revising and improving this paper.

CONFLICT OF INTEREST

The authors declare no conflict of interest.

REFERENCES

ABD MANAN TSB, KHAN T, SIVAPALAN S, JUSOH H, SAPARI N, SARWONO A, RAMLI RM, HARIMURTI S, BEDDU S, SADON SN, KAMAL NLM and MALAKAHMAD A (2019) Application of response surface methodology for the optimization of polycyclic aromatic hydrocarbons degradation from potable water using photo-Fenton oxidation process. *Sci. Total Environ.* **665** 196–212. https://doi.org/10.1016/j.scitotenv.2019.02.060

AGHDASINIA H, BAGHERI R, VAHID B and KHATAEE A (2016) Central composite design optimization of pilot plant fluidized-bed heterogeneous Fenton process for degradation of an azo dye. *Environ. Technol.* **37** (21) 2703–2712. https://doi.org/10.1080/09593330.2016.1159734

ALMEIDA LNB, JOSU TG, FIDELIS MZ, ABREU E, BECHLIN MA, DOS SANTOS OAA and LENZI GG (2021) Process comparison for caffeine degradation: Fenton, photo-Fenton, UV/H_2O_2 and UV/Fe^{3+}. *Water Air Soil Pollut.* **232** (4). https://doi.org/10.1007/s11270-021-05115-1

GIANNAKIS S, LIN K Y A and GHANBARI F. (2021) A review of the recent advances on the treatment of industrial wastewaters by sulfate radical-based advanced oxidation processes(SR-AOPs). *Chem. Eng. J.* **406** 127083. https://doi.org/10.1016/j.cej.2020.127083

BEN HAFAIEDH N, FOURCADE F, BELLAKHAL N and AMRANE A (2020) Iron oxide nanoparticles as heterogeneous electro-Fenton catalysts for the removal of AR18 azo dye. *Environ. Technol.* **41** (16) 2146–2153. https://doi.org/10.1080/09593330.2018.1557258

CHANG Y, CHO Y-C and LIN Y-P (2020) Degradation of PFOS by a MnO_2/H_2O_2 process. *Environ. Sci. Water Res. Technol.* **6** (12) 3476–3487. https://doi.org/10.1039/d0ew00739k

CHEN Z, FU M, YUAN C, HU X, BAI J, PAN R, LU P and TANG M (2021) Study on the degradation of tetracycline in wastewater by micro-nano bubbles activated hydrogen peroxide. *Environ. Technol.* **43** (23) 3580–3590. https://doi.org/10.1080/09593330.2021.1928292

DIAO ZH and CHU W (2021) FeS_2 assisted degradation of atrazine by bentonite-supported nZVI coupling with hydrogen peroxide process in water: Performance and mechanism. *Sci. Total Environ.* **754** 142155. https://doi.org/10.1016/j.scitotenv.2020.142155

DOMINGUES FS, FREITAS T, DE ALMEIDA CA, DE SOUZA RP, AMBROSIO E, PALACIO SM and GARCIA JC (2019) Hydrogen peroxide-assisted photocatalytic degradation of textile wastewater using titanium dioxide and zinc oxide. *Environ. Technol.* **40** (10) 1223–1232. https://doi.org/10.1080/09593330.2017.1418913

DONG H, WANG B, LI L, WANG Y, NING Q, TIAN R, LI R, CHEN J and XIE Q (2019) Activation of persulfate and hydrogen peroxide by using sulfide-modified nanoscale zero-valent iron for oxidative degradation of sulfamethazine: A comparative study. *Sep. Purif. Technol.* **218** 113–119. https://doi.org/10.1016/j.seppur.2019.02.052

DOS SANTOS NO, TEIXEIRA LA, ZHOU Q, BURKE G and CAMPOS L (2021) Fenton pre-oxidation of natural organic matter in drinking water treatment through the application of iron nails. *Environ. Technol.* **43** (17) 2590–2603. https://doi.org/10.1080/09593330.2021.1890838

DULOVA N, KATTEL E and TRAPIDO M (2017) Degradation of naproxen by ferrous ion-activated hydrogen peroxide, persulfate and combined hydrogen peroxide/persulfate processes: The effect of citric acid addition. *Chem. Eng. J.* **318** 254–263. https://doi.org/10.1016/j.cej.2016.07.006

SHIYANG XIA, ZILING SONG, XIAOLIANG ZHAO and JIYANG LI (2023) Review of the recent advances in the prevention, treatment, and resource recovery of acid mine wastewater discharged in coal mines. *J. Water Process Eng.* **52** 2214–7144. https://doi.org/10.1016/j.jwpe.2023.103555

EBRU T, EMMANUEL LKECHUKWU U, EY P S and ZEYNI A (2023) Application of biopolymer in turbidity removal and sludge settling behaviour of travertine-processing wastewater: Performance optimization using response surface methodology (RSM). *Water SA* **49** (1 January). https://doi.org/10.17159/wsa/2023.v49.i1.3952

GAO Y, LI Z, FU Z, ZHANG H, WANG G and ZHOU H (2021) Highly selective capacitive deionization of copper ions in FeS_2@N, S co-doped carbon electrode from wastewater. *Sep. Purif. Technol.* **262** 118336. https://doi.org/10.1016/j.seppur.2021.118336

GOROZABEL-MENDOZA ML, FILHO OAE, ZAMBRANO-INTRIAGO LA, BAQUERIZO-CRESPO RJ, GILER-MOLINA JM and RODRIGUEZ-D AZ JM (2021) Degradation of Blue 1 and Yellow 6 Dyes in binary mixture using photo-Fenton/sunlight system: optimization by factorial designs. *Water Air Soil Pollut.* **232** (12). https://doi.org/10.1007/s11270-021-05461-0

GU C, HU J, ZHANG M, DING J, GONG T, WANG Z, ZHU J and GAN M (2021) Development of a hydroxyl group-mediated biosynthetic schwertmannite as a persulfate activator for efficient degradation of RhB and Cr(VI) removal. *J. Hazardous Mater.* **419** 126496. https://doi.org/10.1016/j.jhazmat.2021.126496

GUO S, WANG Q, LUO C, YAO J, QIU Z and LI Q (2020) Hydroxyl radical-based and sulfate radical-based photocatalytic advanced oxidation processes for treatment of refractory organic matter in semi-aerobic aged refuse biofilter effluent arising from treating landfill leachate. *Chemosphere* 243 125390. https://doi.org/10.1016/j.chemosphere.2019.125390

HAJI S, BENSTAALI B and AL-BASTAKI N (2011) Degradation of methyl orange by UV/H_2O_2 advanced oxidation process. *Chem. Eng. J.* **168** (1) 134–139. https://doi.org/10.1016/j.cej.2010.12.050

HAJI S, KHALAF M, SHUKRALLAH M, ABDULLAH J and AHMED S (2014) A kinetic comparative study of azo dye decolorization by catalytic wet peroxide oxidation using Fe–Y zeolite/H_2O_2 and photooxidation using UV/H_2O_2. *Reaction Kinetics, Mech. Catal.* **114** (2) 795–815. https://doi.org/10.1007/s11144-014-0810-3

HAMAD D, DHIB R and MEHRVAR M (2016) Effects of hydrogen peroxide feeding strategies on the photochemical degradation of polyvinyl alcohol. *Environ. Technol.* **37** (21) 2731–2742. https://doi.org/10.1080/09593330.2016.1160959

JIANG Y, SUN D, WANG D, TONG L, ZHANG Z, CAO N and GONG Z (2021) Rapid degradation of tetracycline in aqueous solution by Fe/Cu catalysis enhanced by H_2O_2 activation. *Environ. Technol.* **43** (24) 1–9. https://doi.org/10.1080/09593330.2021.1933610

JIN X, SU J and YANG Q (2021) A comparison study of Fenton-like and Fenton reactions in dichloromethane removal. *Environ. Technol.* **9**: 1–11. https://doi.org/10.1080/09593330.2021.1954096

KAYAN I, OZ NA and KANTAR C (2020) Coupling pyrite-Fenton process with aerobic biodegradation for the treatment of 2-chlorophenol. *Water Air Soil Pollut.* **231** (9). https://doi.org/10.1007/s11270-020-04836-z

KOKILAVANI S, SYED A, RAJU LL, AL-RASHED S, ELGORBAN AM, THOMAS AM and KHAN SS (2021) Synthesis of novel heterostructured FeS_2/Ag_2MoO_4 nanocomposite: Characterization, efficient antibacterial and enhanced visible light driven photocatalytic activity. *Surf. Interf.* **23** 101003. https://doi.org/10.1016/j.surfin.2021.101003

LI L, LAI C, HUANG F, CHENG M, ZENG G, HUANG D, LI B, LIU S, ZHANG M, QIN L, LI M, HE J, ZHANG Y and CHEN L (2019) Degradation of naphthalene with magnetic bio-char activate hydrogen peroxide: Synergism of bio-char and Fe-Mn binary oxides. *Water Res.* **160** 238–248. https://doi.org/10.1016/j.watres.2019.05.081

LIU H, FU P, LIU F, HOU Q, TONG Z and BI W (2022) Degradation of ciprofloxacin by persulfate activated with pyrite: mechanism, acidification and tailwater reuse. *RSC Adv.* **12** (46) 29991–30000. https://doi.org/10.1039/d2ra05412d

LIU H, LIU F, ZHANG J, ZHOU J, BI W, QIN J, HOU Q, NI Y, XU S and YANG C (2022) Degradation of methyl orange by pyrite activated persulfate oxidation: mechanism, pathway and influences of water substrates. *Water Sci. Technol.* **85** (10) 2912–2927. https://doi.org/10.2166/wst.2022.134

LIU T, CHEN N, DENG Y, CHEN F and FENG C (2020) Degradation of p-nitrophenol by nano-pyrite catalyzed Fenton reaction with enhanced peroxide utilization. *RSC Adv.* **10** (27) 15901–15912. https://doi.org/10.1039/d0ra01177k

LIU W, WANG Y, AI Z and ZHANG L (2015) Hydrothermal synthesis of FeS_2 as a high-efficiency fenton reagent to degrade alachlor via superoxide-mediated Fe(II)/Fe(III) Cycle. *ACS Appl. Mater. Interfaces* **7** (51) 28534–28544. https://doi.org/10.1021/acsami.5b09919

LIU Y, ZHAO Y and WANG J (2021) Fenton/Fenton-like processes with in-situ production of hydrogen peroxide/hydroxyl radical for degradation of emerging contaminants: Advances and prospects. *J. Hazardous Mater.* **404** (Pt B) 124191. https://doi.org/10.1016/j.jhazmat.2020.124191

MA X, CHENG Y, GE Y, WU H, LI Q, GAO N and DENG J (2018) Ultrasound-enhanced nanosized zero-valent copper activation of hydrogen peroxide for the degradation of norfloxacin. *Ultrasonics Sonochem.* **40** (Pt A) 763–772. https://doi.org/10.1016/j.ultsonch.2017.08.025

MARTINS A, TEIXEIRA LAC, DA FONSECA FV and YOKOYAMA L (2017) Evaluation of the mercaptobenzothiazole degradation by combined adsorption process and Fenton reaction using iron mining residue. *Environ. Technol.* **38** (16) 2032–2039. https://doi.org/10.1080/09593330.2016.1244571

ORAL O and KANTAR C (2019) Diclofenac removal by pyrite-Fenton process: Performance in batch and fixed-bed continuous flow systems. *Sci. Total Environ.* **664** 817–823. https://doi.org/10.1016/j.scitotenv.2019.02.084

PENG J, ZHANG Y, ZHANG C, MIAO D, LI J, LIU H, WANG L and GAO S (2019) Removal of triclosan in a Fenton-like system mediated by graphene oxide: Reaction kinetics and ecotoxicity evaluation. *Sci. Total Environ.* **673** 726–733. https://doi.org/10.1016/j.scitotenv.2019.03.354

PINEDO-HERNANDEZ S, SÁNCHEZ-MENDIETA V, SOLACHE-RÍOS M and GUTIRREZ-SEGURA E (2022) Degradation of brilliant blue by heterogeneous Fenton and UV-fenton processes. *Water Air Soil Pollut.* **233** (7). https://doi.org/10.1007/s11270-022-05722-6

SHAO P, YU S, DUAN X, YANG L, SHI H, DING L, TIAN J, YANG L, LUO X and WANG S (2020) Potential difference driving electron transfer via defective carbon nanotubes toward selective oxidation of organic micropollutants. *Environ. Sci. Technol.* **54** (13) 8464-8472. https://doi.org/10.1021/acs.est.0c02645

SHUKLA N and REMYA N (2021) Microwave photo-oxidation with diverse oxidants for Congo red degradation: effect of oxidants, degradation pathway and economic analysis. *Environ. Technol.* **42** (10) 1482–1492. https://doi.org/10.1080/09593330.2019.1670737

SONG W, LI J, ZHANG X, FENG J, DU X, WANG Q, FU C, QIU W, WANG Z and GAO X (2022) A feasible approach for azo-dye methyl orange degradation in siderite/H_2O_2 assisted by persulfate: Optimization using response surface methodology and pathway. *J. Environ. Manage.* **308** 114397. https://doi.org/10.1016/j.jenvman.2021.114397

SUAVE J, JOSE HJ and MOREIRA R (2018) Photocatalytic degradation of polyvinylpyrrolidone in aqueous solution using TiO_2/H_2O_2/UV system. *Environ. Technol.* **39** (11) 1404–1412. https://doi.org/10.1080/09593330.2017.1330365

SUN Y, CHO DW, GRAHAM NJD, HOU D, YIP ACK, KHAN E, SONG H, LI Y and TSANG DCW (2019) Degradation of antibiotics by modified vacuum-UV based processes: Mechanistic consequences of H_2O_2 and $K_2S_2O_8$ in the presence of halide ions. *Sci. Total Environ.* **664** 312–321. https://doi.org/10.1016/j.scitotenv.2019.02.006

TANG J and WANG J (2017) Fe-based metal organic framework/graphene oxide composite as an efficient catalyst for Fenton-like degradation of methyl orange. *RSC Adv.* **7** (80) 50829–50837. https://doi.org/10.1039/c7ra10145g

WANG C, SUN R, HUANG R and CAO Y (2021) A novel strategy for enhancing heterogeneous Fenton degradation of dye wastewater using natural pyrite: Kinetics and mechanism. *Chemosphere* **272** 129883. https://doi.org/10.1016/j.chemosphere.2021.129883

WANG WM, SONG J and HAN X (2013) Schwertmannite as a new Fenton-like catalyst in the oxidation of phenol by H_2O_2. *J. Hazardous Mater.* **262** 412–419. https://doi.org/10.1016/j.jhazmat.2013.08.076

XIAO R, HE L, LUO Z, SPINNEY R, WEI Z, DIONYSIOU DD and ZHAO F (2020) An experimental and theoretical study on the degradation of clonidine by hydroxyl and sulfate radicals. *Sci. Total Environ.* **710** 136333. https://doi.org/10.1016/j.scitotenv.2019.136333

XU H and SHENG Y (2021) New insights into the degradation of chloramphenicol and fluoroquinolone antibiotics by peroxymonosulfate activated with FeS: Performance and mechanism. *Chem. Eng. J.* **414** 128823. https://doi.org/10.1016/j.cej.2021.128823

YAN J, QIAN L, GAO W, CHEN Y, OUYANG D and CHEN M (2017) Enhanced Fenton-like degradation of trichloroethylene by hydrogen peroxide activated with nanoscale zero valent iron loaded on biochar. *Sci. Rep.* **7** 43051. https://doi.org/10.1038/srep43051

YE J, ZANG Y, WANG Q, ZHANG Y, SUN D, ZHANG L, WANG G, ZHENG X and ZHU J (2021) Nitrogen doped FeS_2 nanoparticles for efficient and stable hydrogen evolution reaction. *J. Energ. Chem.* **56** 283–289. https://doi.org/10.1016/j.jechem.2020.08.014

YOUSSEF NA, SHABAN SA, IBRAHIM FA and MAHMOUD AS (2016) Degradation of methyl orange using Fenton catalytic reaction. *Egyptian J. Petrol.* **25** (3) 317–321. https://doi.org/10.1016/j.ejpe.2015.07.017

YU F, WANG Y, MA H and ZHOU M (2020) Hydrothermal synthesis of FeS_2 as a highly efficient heterogeneous electro-Fenton catalyst to degrade diclofenac via molecular oxygen effects for Fe(II)/Fe(III) cycle. *Sep. Purif. Technol.* **248** 117022. https://doi.org/10.1016/j.seppur.2020.117022

ZHANG X, QIN Y, ZHANG W, ZHANG Y and YUAN GE (2020) Oxidative degradation of Orange G in aqueous solution by persulfate activated with pyrite. *Water Sci. Technol.* **82** (1) 185–193. https://doi.org/10.2166/wst.2020.352

ZHAO Z, PAN S, YE Y, ZHANG X and PAN B (2020) FeS_2/H_2O_2 mediated water decontamination from p-arsanilic acid via coupling oxidation, adsorption and coagulation: Performance and mechanism. *Chem. Eng. J.* **381** 122667. https://doi.org/10.1016/j.cej.2019.122667

ZHIYONG Y, WENHUA W, LIN S, LIQIN L, ZHIYIN W, XUANFENG J, CHAONAN D and RUIYING Q (2013) Acceleration comparison between Fe^{2+}/H_2O_2 and Co^{2+}/oxone for decolouration of azo dyes in homogeneous systems. *Chem. Eng. J.* **234** 475–483. https://doi.org/10.1016/j.cej.2013.08.013

APPENDIX

Table A1. Physical and chemical properties of different water matrices

Physicochemical property	Tap water	River water
Water temperature	18.3°C	19.6°C
pH	7.69	7.97
Electrical conductivity	535 µS/cm	655 µS/cm
TOC	8.17 mg/L	13.62 mg/L
Na^+	14.13 mg/L	11.51 mg/L
K^+	1.95 mg/L	3.70 mg/L
Ca^{2+}	18.04 mg/L	12.02 mg/L
Mg^{2+}	74.13 mg/L	55.90 mg/L
Cl^{2-}	53.18 mg/L	39.88 mg/L
HCO_3^-	292.88 mg/L	289.83 mg/L
SO_4^{2-}	214.20 mg/L	406.32 mg/L

Note: The river water was taken from the Wuma River, Taigu, Jinzhong City, Shanxi Province on 26 November 2020 (37°27′11″ N, 112°33′18″ E)

Table A2. FeS_2/H_2O_2 system degrades methyl orange intermediates

Products	m/z	Structural formula
MO	327.07	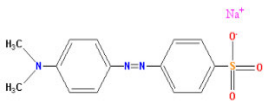
P1	276.04	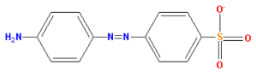
P2	306.09	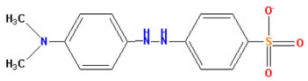
P3	157.00	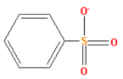
P4	136.10	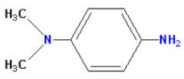
P5	290.06	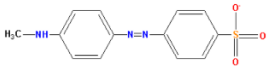
P6	261.03	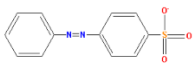
P7	187.02	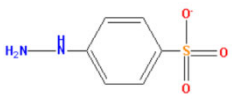
P8	172.01	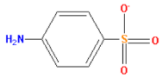

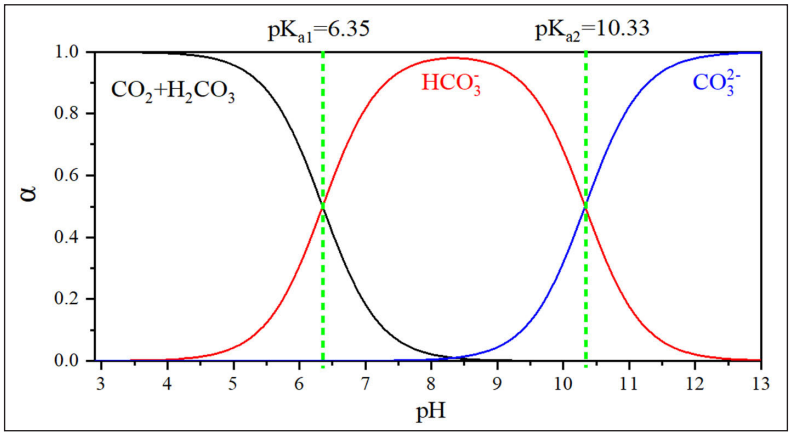

Figure A1. Carbonation binding state distribution diagram

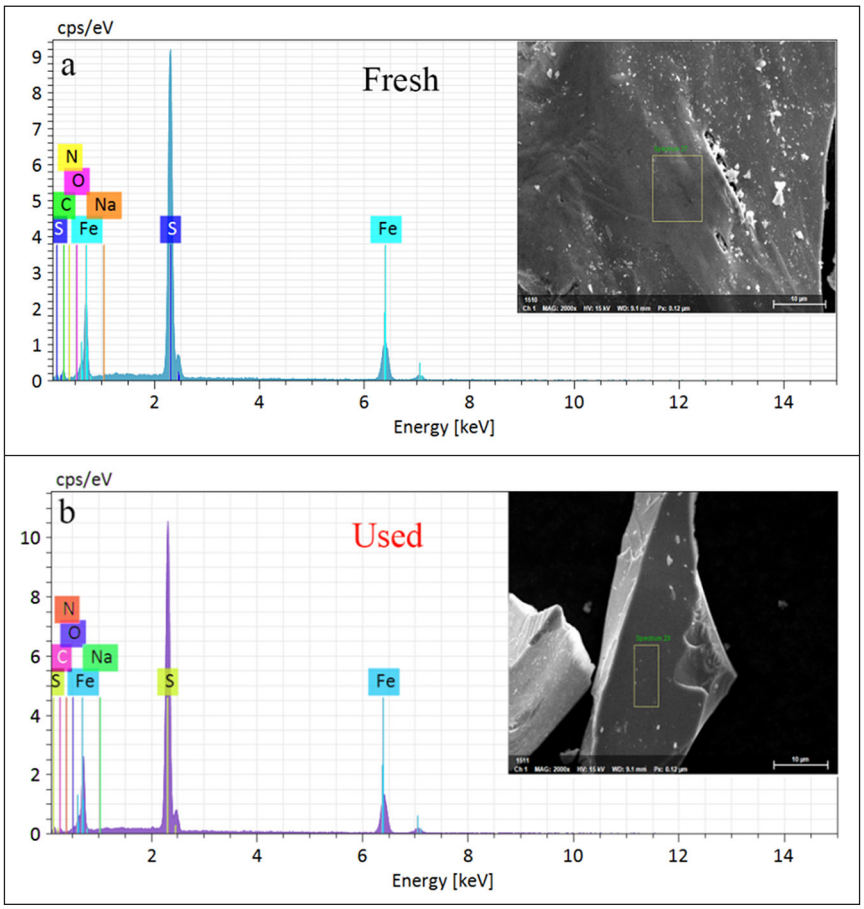

Figure A2. SEM and EDS spectra of (a) fresh and (b) used pyrite

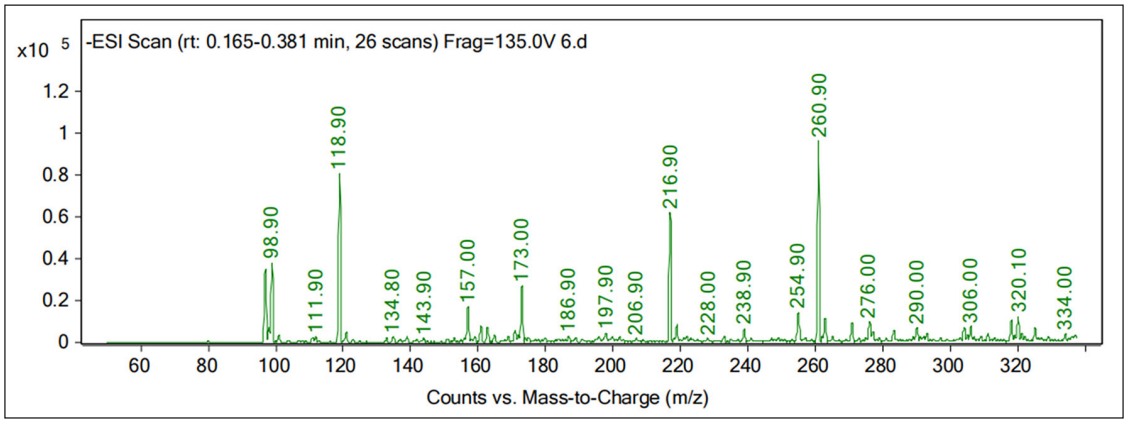

Figure A3. Analysis results of LC-MS(ESI-) degradation products